Measurement of Cloud Droplet Size Spectra by Doppler Radar

EARL E. GOSSARD

Cooperative Institute for Research in Environmental Sciences (CIRES), University of Colorado, Boulder, Colorado

(Manuscript received 15 June 1993, in final form 17 November 1993)

ABSTRACT

A new technique is examined for using Doppler radars to extract information about the size spectrum of cloud droplets too small to have terminal velocities large enough to be resolvable by the radar. If the drops are very small, motions of the drops are dominated by turbulent fluctuations in the medium rather than their fall velocity. Their motion is then the convolution of the terminal velocity with the turbulent velocity probability density function, and size information about the population can be obtained only by deconvolving the spectra. Doppler radars can extract this velocity and size information, as well as cloud liquid and liquid flux, using a surprisingly simple and accurate technique assuming some functional form (e.g., gamma) for the drop number density spectrum. The method also allows Doppler radars to extract drop size information independent of up-/downdrafts in the medium in which they are embedded. Various gamma and lognormal functions are compared, and finally, a "Stokes range" of drop sizes is added and found to be important. Examples are shown and errors are discussed.

1. Introduction

It has been well established that vertically pointing Doppler radars can be used effectively to measure remotely the drop size distribution of precipitating particles in clouds. The basic technique is old, and early work is summarized by Atlas et al. (1973). A major drawback of the technique at that time was the contaminating motions of the atmospheric medium in which the drops were embedded, such as up-/downdrafts and turbulence. The use of the new "clear-air" wind profilers to measure Doppler spectra of precipitating particles allows most of the contamination related to the medium to be removed, because long-wavelength radars sense the spectral band of the atmospheric medium separately from the precipitation band. Then the up-/downdraft can be removed and turbulence effects minimized by deconvolution (Wakasugi et al. 1986; Gossard and Strauch 1989; Gossard et al. 1990). In all of that work, the size information about the drop population was deduced from direct terminal velocity spectra observed by vertically pointing radars. [Here we adopt the convention used in Doviak and Zrnić (1984) and define "terminal" velocity to mean the fall velocity relative to the medium, i.e., after the up-/downdrafts have been removed.] When the settling velocity of cloud droplets was too small to be resolvable in the radar spectra, the technique was not effective. In this paper we describe a technique capable of extracting crucial size information even in the cloud portion of the spectrum.

The measured spectrum is the convolution of the "quiet-air" Doppler fall velocity (i.e., terminal velocity) spectrum with the turbulent velocity probability density function (PDF), which is usually assumed to be Gaussian. To recover the quiet-air spectrum, we must therefore deconvolve the radar-measured spectrum and the turbulence PDF. The velocity resolution provided by practical radars yields too few sample points for accurate deconvolution by Fourier transformation or by the various iterative schemes. Even with careful windowing, large artificial perturbations can be introduced near the ends of the sample (Gossard and Strauch 1990). Furthermore, any unwanted noise perturbations in the sample may be greatly enhanced by the deconvolution process. We, therefore, find an exact deconvolution for a gamma distribution using an exponential PDF for which integrations can be performed analytically. This analytical deconvolution is then compared with corresponding numerical solutions that use a more realistic Gaussian PDF, and with a lognormal distribution rather than a gamma distribution. The calculations are then carried out with and without a "Stokes range" of velocities.

2. Some fundamental relations

Most radar observations since Marshall and Palmer (1948) suggest that the drop size versus number density spectra can be well represented by one or more exponential regimes. We first consider gamma functions, for which the exponential function is a simple special

Corresponding author address: Dr. Earl E. Gossard, CIRES, Box 449, University of Colorado, Boulder, CO 80309.

case. In formulating the problem, we follow the development by Gossard et al. (1990). We begin by noting that the radar reflectivity factor Z is related to drop diameter D and drop number density $N(D)$ by

$$Z = \int_0^\infty N(D)D^6 dD; \tag{1}$$

therefore, the spectral density of Z is

$$S_Z(D) = N(D)D^6. \tag{2}$$

If $N(D)$ has a modified gamma distribution, say,

$$N(D) = B\left(\frac{D}{D_g}\right)^\alpha \exp\left[-\left(\frac{D - D_g}{D_g}\right)\right], \tag{3}$$

then (2) gives

$$S_Z(D) = BD_g^6\left(\frac{D}{D_g}\right)^{6+\alpha} \exp\left[-\left(\frac{D - D_g}{D_g}\right)\right], \tag{4}$$

where B is a proportionality constant and D_g is a length scale allowing the maximum in $S_Z(D)$ to be positioned at will; that is, if D_M is the diameter at the maximum of the function, $D_g = D_M/(6 + \alpha)$. Thus, if a value of D_M is indicated by an observed spectral maximum in Z, D_g is readily calculated for any assumed α. It is convenient to use (4) in a form normalized to the values S_M, N_M, and D_M at the maximum of the function (e.g., Atlas et al. 1973; Gossard et al. 1990), so that

$$S_Z(D) = S_M\left(\frac{D}{D_M}\right)^{6+\alpha} \exp\left[(6 + \alpha)\left(1 - \frac{D}{D_M}\right)\right] \tag{5}$$

and

$$N(D) = N_M\left(\frac{D}{D_M}\right)^{\alpha} \exp\left[(6 + \alpha)\left(1 - \frac{D}{D_m}\right)\right], \tag{6}$$

where $N_M = S_M D_M^{-6}$ is the number density at the maximum of the S_Z function. Thus when $\alpha = 0$, $N(D)$ is just distributed exponentially.

Doppler radars actually measure spectra of reflectivity versus droplet vertical velocity w rather than size D. If we can correctly calculate the number density distribution $N(D)$ from the measured $S_Z(w)$, we can find the cloud liquid mass distribution $M(D)$ from

$$M(D) = \rho_w \frac{\pi}{6} N(D)D^3 \tag{7}$$

and the liquid flux (or precipitation rate) spectrum $F(D)$ from

$$F(D) = M(D)w(D). \tag{8}$$

The size scale D_M is easily related to the more familiar (e.g., Atlas 1953) liquid mass median diameter D_0 for an exponential distribution ($\alpha = 0$) by

$$D_\alpha = \frac{3.67 + \alpha}{6 + \alpha} D_M, \tag{9}$$

where D_α is the droplet mass (or volume) median diameter for a gamma distribution of given α. When $\alpha = 0$ (exponential), $D_\alpha = D_0 = (3.67/6)D_M$. The advantage of using D_M in analyzing radar data is that it is quickly identifiable in real time in the spectral displays and in the linear range is "slide-rule" convertible to the corresponding modes of the liquid mass and number density distributions.

Figure 1 gives terminal velocities of drops in quiet air (V_f) versus drop size (Gunn and Kinzer 1949; Foote and du Toit 1969). The asterisk points are measured values at 1013 mb from Table B1 of Mason (1971). The curves were determined from commonly used theoretical functions (e.g., Beard 1985; Rogers and Yau 1989).

The solid curves represent the function

$$D(\text{mm}) = 0.25\left(\frac{\rho}{\rho_0}\right)^{0.5} V_f, \tag{10a}$$

which is applicable for $V_f \leqslant 2.5$ m s^{-1}. It is shown for three cloud altitudes corresponding to air densities ρ at pressure levels of 1013 (MSL), 840, and 700 mb. A power of 0.4 rather than 0.5 on ρ/ρ_0 was found by Foote and du Toit (1969) and Beard (1985) because the larger drops depart from sphericity. We will therefore use 0.4 for the larger drops.

The dashed curve shows the function (e.g., see Atlas et al. 1973)

$$D\,(\text{mm}) = -1.667 \ln\left[\frac{9.65 - V_f(\rho/\rho_0)^{0.4}}{10.3}\right], \tag{10b}$$

which is applicable for $V_f > 2.5$ m s^{-1}, plotted for an air density corresponding to 1013 mb.

For the moment, we have ignored the Stokes range of very small drops ($V_f < 0.5$ m s^{-1}) and will examine the drop size range for which the linear relationship (10a) applies in quiet air. (We examine the effect of the Stokes range in the final section where we consider small drop populations.) For droplets embedded in a real atmosphere, turbulence and/or up-/downdrafts may have a large effect, and the actual observed vertical velocity w must be represented as a distribution about the mean settling velocity given by (10a). Thus the observed reflectivity spectrum is the convolution of the quiet-air reflectivity, $S_{QZ}(V_f)$, with the turbulent PDF (Gossard and Strauch 1989), where the subscript Q designates the quiet-air function.

3. Deconvolving cloud spectra

The general considerations in deconvolving Doppler velocity spectra to obtain size spectra have been discussed by Gossard and Strauch (1990). Direct deconvolution of the Doppler spectra by iteration or by Fourier transformation requires great care in windowing to remove short-sample artifacts and in removing unwanted spectral noise. The technique treats all pertur-

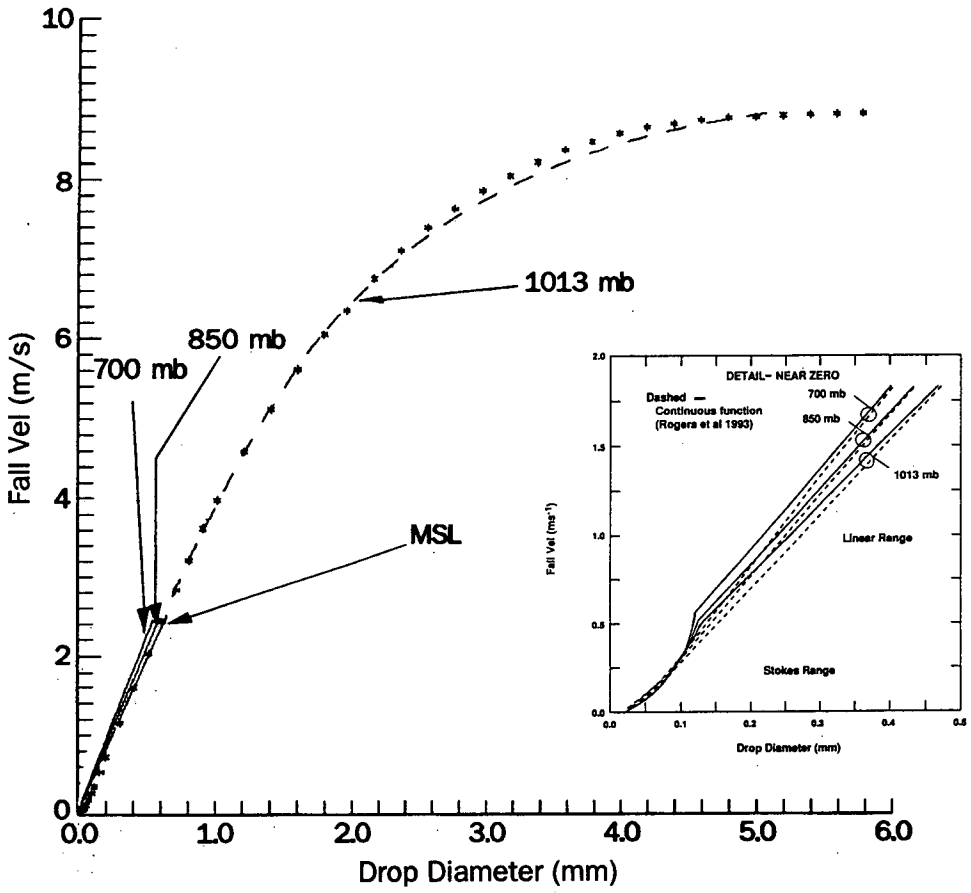

FIG. 1. Quiet-air terminal fall velocity versus water drop diameter. Asterisk points are from Table B1 of Mason (1971). The solid curves represent the function given by Eq. (10a); the dashed curve represents the function given by Eq. (10b).

bations as real and smoothed by turbulence, so the noise features are enhanced as are the wanted lines. When the deconvolution effect is small, as is often true for precipitating drops for which V_f is much greater than the turbulent velocity fluctuations, the noise enhancement is not serious (Gossard et al. 1990), but in the present application the deconvolution effect is large. Therefore we choose to deconvolve various proposed theoretical functions, and we describe an analytical solution that does not involve Fourier transformation or iteration, which we then compare with various numerical results. For convenience in the integrations we first chose an exponential PDF given by

$$\text{PDF} = \frac{1}{2w_\sigma} \exp\left[-\left(\frac{|w - w_i|}{w_\sigma}\right)\right], \qquad (11)$$

where w_σ is the half-width to the e^{-1} point of the distribution. Suppose we consider one resolution interval, Δw, at w_i in the quiet-air spectrum shown in Fig. 2. If turbulence is imposed on such a quiet-air spectral line, its power is shown spread over the shaded area. It is clear that the turbulent line strength at w_j is reduced to $\Delta w(2w_\sigma)^{-1} S_Q(w_i)$ and the variance density of vertical velocity w is distributed exponentially over neighboring lines. Thus for a continuous quiet-air spectrum, whose number density and reflectivity are of the forms (5) and (6), the Doppler spectrum measured by the radar at any line w_i will be the sum of contributions from all lines in the spectrum weighted exponentially over the distance they are separated from the line in question. Formally, the spectral density of Z is

$$S_Z(w_i)\Delta w = \frac{\Delta w}{2w_\sigma} \int_0^\infty S_Q(w_j) \times \exp\left[-\left(\frac{|w_j - w_i|}{w_\sigma}\right)\right] dw_j \qquad (12a)$$

or

$$S_Z(w_i) = \frac{1}{2w_\sigma}\left[\int_0^{w_i} S_Q(w_j) \exp\left(\frac{w_j - w_i}{w_\sigma}\right) dw_j + \int_{w_i}^\infty S_Q(w_j) \exp\left(\frac{w_i - w_j}{w_\sigma}\right) dw_j\right]. \qquad (12b)$$

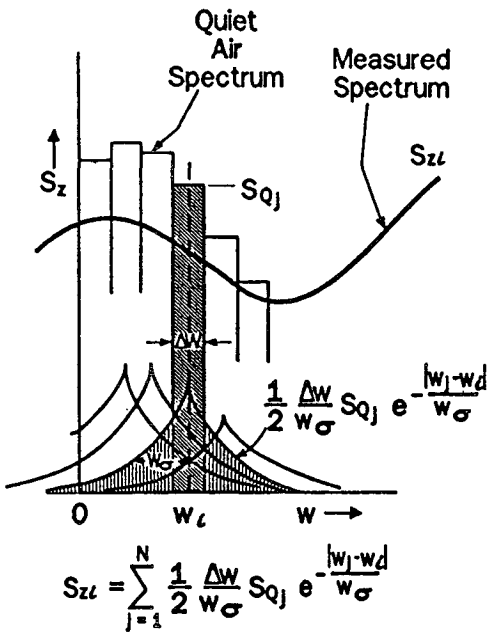

FIG. 2. Schematic description of the effect of atmospheric turbulence on the Doppler spectrum of falling drops.

For small drops, (10a) shows that the terminal fall velocity is essentially a linear function of D (say, $D = kw_j$), so $S_Q(w_j)$ has the same form as (5), and (12a) and (12b) can be simply integrated. Truncation of the integrals is not considered here.

Using (5) for $S_Q(w_j)$, and transforming variables, letting $x = w_j/w_M$ and $n = 6 + \alpha$, where n is an integer, the first integral in (12b) becomes

$$S_{Z1}(w_i) = S_{QM}\left(\frac{1}{2w_\sigma}\right)\exp\left(n - \frac{x_i}{y}\right) w_M I_a(x_i), \quad (13)$$

where

$$I_a(x_i) = \int_0^{x_i} x_j^n \exp(ax_j)dx_j,$$

w_M is the terminal fall velocity V_f at the maximum of $S_Q(w_j) \equiv S_{QM}$:

$$a = -6 - \alpha + \frac{w_M}{w_\sigma} \equiv -n + \frac{1}{y},$$

$$x_j = \frac{w_j}{w_M},$$

$$x_i = \frac{w_i}{w_M},$$

$$y = \frac{w_\sigma}{w_M}.$$

The second integral in (12b) becomes

$$S_{Z2}(w_i) = S_{QM}\left(\frac{1}{2w_\sigma}\right)\exp\left(n + \frac{x_i}{y}\right) w_M I_b(x_i), \quad (14)$$

where

$$I_b(x_i) = \int_{x_i}^{\infty} x_j^n \exp(bx_j)dx_j,$$

$$b = -6 - \alpha - \frac{w_M}{w_\sigma} \equiv -n - \frac{1}{y}.$$

For $wi < 0$ we proceed by noting that $w_j > 0$, so $w_j > w_i$. The integral is then simply

$$S_{Z3}(w_i) = S_{QM}\left(\frac{1}{2w_\sigma}\right)\exp\left(n + \frac{x_i}{y}\right) w_M I_0, \quad (15)$$

where

$$I_0 = \int_0^{\infty} x_j^n \exp(bx_j)dx_j = \frac{n!}{b^{n+1}}$$

and I_a and I_b are the incomplete gamma function. For noninteger powers (n), tables of the integral may be found in Pearson (1951) or in appendix C of Gossard and Strauch (1983). For integer powers the integrations are simple but tedious; that is,

$$I_a(x_i) = \exp(ax_i)E_1(x_i) \pm \frac{n!}{a^{n+1}}. \quad (16)$$

If a is negative, the negative sign on the last term is chosen if n is even, and the positive sign if n is odd. Also

$$I_b(x_i) = -\exp(bx_i)E_2(x_i), \quad (17)$$

where the expansion E is

$$E_{1,2}(x_i) = \frac{x_i^n}{c} - \frac{n}{c^2}x_i^{n-1} + \frac{n(n-1)}{c^3}x_i^{n-2} - \frac{n(n-1)(n-2)}{c^4}x_i^{n-3} \cdots \frac{n!}{c^{n+1}}, \quad (18)$$

where $c = a$ for E_1 in (16), and $c = b$ for E_2 in (17). Then

$$S_{Z1}(x_i) = S_{QM}\left(\frac{w_M}{2w_\sigma}\right)\exp\left(-\frac{w_i}{w_\sigma}\right)\exp(n)I_a(x_i), \quad (19)$$

$$S_{Z2}(x_i) = S_{QM}\left(\frac{w_M}{2w_\sigma}\right)\exp\left(\frac{w_i}{w_\sigma}\right)\exp(n)I_b(x_i), \quad (20)$$

$$S_{Z3}(x_i) = S_{QM}\left(\frac{w_M}{2w_\sigma}\right)\exp\left(\frac{w_i}{w_\sigma}\right)\exp(n)I_0, \quad \text{for } w_i < 0. \quad (21)$$

Therefore, the spectrum of the turbulence-convolved $S_Z(x_i)$ is

$$S_Z(x_i) = S_{Z1}(x_i) + S_{Z2}(x_i), \quad \text{for } x_i > 0 \quad (22a)$$

$$S_Z(x_i) = S_{Z3}(x_i), \quad \text{for } x_i \leq 0. \quad (22b)$$

Convolved spectra of S_Z for several w_σ values are shown in Fig. 3. The deconvolution factor (DF), that is, the ratio of the peak of the deconvolved (quiet air) spectrum to the peak of the turbulence-convolved spectrum, is plotted in Fig. 4. Noting that $S_Z(w_i)dw_i = S_Z(D)dD$, we use the maximum $S_Z(w_i)$, found from (22a), for the quiet-air value of S_M in (5).

Taking the derivative of (22a), and applying L'Hospital's rule to get x_m (and w_m) at the spectral maximum (indicated by lower case m), we find the equality

$$-(n+a)I_a(x_m) + (n+b)I_b(x_m) = -\frac{w_m}{w_\sigma}\frac{n!}{a^{n+1}}\exp(-ax_m) \quad (23)$$

for which the relevant roots lie near $x \equiv w_m/w_M = 1$. For an exponential PDF, the convolved maximum shifts very little from $x_i = 1$. (For $2w_\sigma/w_M = 5$, x_i is only 1.1; i.e., $w_m = w_M$.) This offers procedural simplification because for most purposes $E_{1,2}$ need only be evaluated at $x_i = 1$.

Because Doppler radars can measure the maximum value of the Z spectrum $[S_Z(w_m)]$ and can, in principle, measure w_σ from the spectral width of the peak in S_Z near $w = 0$, (22) and (5) yield the deconvolved cloud spectrum when the drop size distribution in the cloud is a gamma function of a given α and when the size versus fall velocity relation is linear.

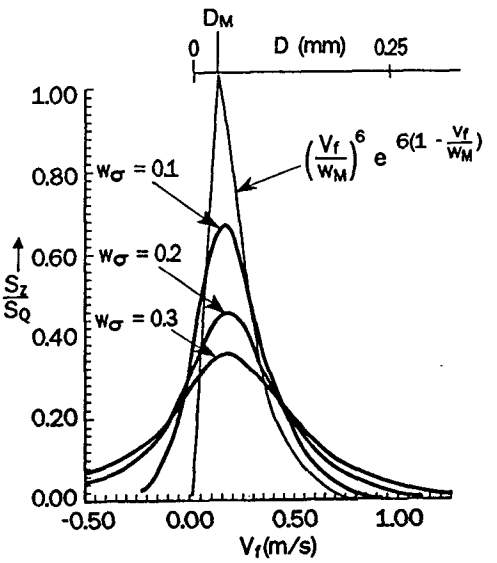

FIG. 3. Calculated Doppler spectra of the radar reflectivity factor, assuming an exponential drop size distribution ($\alpha = 0$) in quiet air (light solid), and the resulting convolved spectra for various turbulent intensities w_σ (dark solid), assuming an exponential PDF (see Fig. 2).

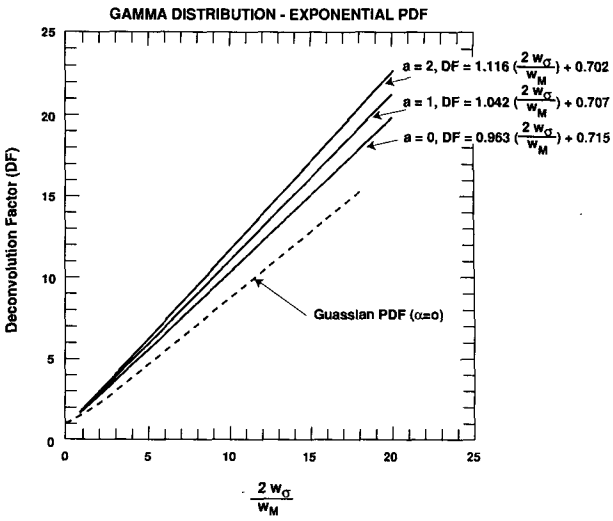

FIG. 4. Deconvolution factors calculated from Eq. (29) for assumed quiet-air number density distributions that are gamma functions with alpha values of 0, 1, and 2 [see Eqs. (5) and (6)].

Equation (5) is easily integrated over all the cloud particles to obtain the total radar reflectivity factor

$$Z_Q = S_{QM}w_M e^{6+\alpha}\frac{(6+\alpha)!}{(6+\alpha)^{7+\alpha}} \equiv \frac{S_{QM}w_m}{[f(\alpha)]}, \quad (24)$$

where S_{QM} is the spectral maximum of the quiet-air spectrum we seek, located where $w_i = w_M$. Equation (24) defines the function $f(\alpha)$ for future convenience. From (6), (7), (8), and (10) we find the cloud density totals of number, liquid mass, and flux to be

$$N_T = \frac{(6+\alpha)^6}{(6+\alpha)!}\alpha!\frac{1}{D_M^6}Z, \quad (25)$$

$$\text{LW} = \rho_W\left(\frac{\pi}{6}\right)\frac{(6+\alpha)^3}{D_M^3}\frac{(3+\alpha)!}{(6+\alpha)!}Z \quad (\text{g m}^{-3}), \quad (26)$$

$$F_T = \rho_W\left(\frac{\pi}{6}\right)w_M\frac{1}{D_M^3}(6+\alpha)^2\frac{(4+\alpha)!}{(6+\alpha)!}Z \quad (\text{g m}^{-2}\,\text{s}^{-1}), \quad (27)$$

where ρ_W is the density of liquid water in grams per cubic millimeter and Z is in its standard units ($\text{mm}^6\ \text{m}^{-3}$) if D is in millimeters.

The fundamental measurable is the spectrum $S_Z(w)$ from which we can calculate the radar reflectivity factor Z [Eq. (1)] and the spectral peak amplitude S_M. Because the total reflectivity Z is independent of the turbulent smear, (24) (with $\alpha = 0$) gives

$$S_{QM}w_M = \frac{Z}{1.037}, \quad (28)$$

which is constant and measurable regardless of the turbulent convolution of the spectrum, so (24) or (28) provides a means of calculating w_M from radar measurements if the measured S_M can be used to get S_{QM}. It remains to calculate S_{QM} and w_M independently for a given turbulence condition.

We note that the ratio of the convolved spectral maximum to the maximum of the quiet-air spectrum is given by $S_z(x_m)/S_{QM}$. We call the inverse of this ratio the deconvolution factor (DF), given by

$$\mathrm{DF}(w_M, w_\sigma) = \frac{S_{QM}}{S_M} = \left[\frac{S_{Z1}(w_M, w_\sigma) + S_{Z2}(w_M, w_\sigma)}{S_{QM}}\right]^{-1}, \quad (29)$$

where M indicates the convolved spectral maximum. Here, DF depends on w_M and w_σ through the constants a and b. (Note that S_{Z3} is irrelevant because w_M is always positive.)

From (24), we note that the calculation of fall velocity does not use the direct measurement of vertical velocity by the radar, and so it is independent of up-/downdrafts. Here, Z and S_m are direct observables and w_σ can be found from the observations, so

$$w_M = [f(\alpha)]\frac{Z}{S_m}\left[\frac{1}{\mathrm{DF}(w_M)}\right]. \quad (30)$$

Although DF depends on w_M, w_M can be found as an implicit solution of (30). For the exponential PDF the technique is greatly facilitated by the fact that the DF (shown plotted in Fig. 4) varies essentially linearly with $2w_\sigma/w_M$ over the range of most interest. The best-fit lines are shown in Fig. 4 for three α's. They are given by

$$\mathrm{DF} = C + [f(\alpha)]\frac{2w_\sigma}{w_M}, \quad (31)$$

where

$$f(\alpha) = \exp[-(6+\alpha)]\frac{(6+\alpha)^{7+\alpha}}{(6+\alpha)!}$$

and

$$C = \frac{1}{1.399 + 0.013\alpha},$$

which inserted into (30) gives

$$w_M = \frac{f(\alpha)}{C}\left(\frac{Z}{S_M} - 2w_\sigma\right). \quad (32)$$

Clear-air turbulent fluctuations of refractive index might be expected to produce a symmetrical $S_Z(w)$ spectrum simply given by the PDF [Eq. (11)]. Integration then gives the apparent $Z/S_M = 2w_\sigma$, which, inserted into (32) gives $w_M = 0$ (i.e., zero fall velocity), as it should. Thus the "settling" velocity given by (32) is a result of the slight spectral asymmetry, extracted by the integration that yields Z, represented by the "bulk" shape parameter Z/S_M, which allows velocity and size information to be extracted for scales much smaller than are usually resolvable in the Doppler velocity spectrum near $w = 0$. It is important to note that the shape parameter is independent of up-/downdrafts, so the velocity–size information is also free of such contamination.

To find w_σ, we note from (21) that when $w_i < 0$ the shape of the spectrum is independent of w_M and simply decreases as $\exp|w_i/w_\sigma|$. Therefore the slope of a regression fit to the log plot of the spectrum S_Z, for $w_i < 0$, provides the estimate of w_σ.

Having w_σ, Z, and S_M from the reflectivity factor spectrum, we can then find w_M from (32); the totals of liquid mass density and flux are found from (26) and (27). Thus, the w_M found by this technique after deconvolution of the spectrum provides the measure of cloud drop size that we need to calculate liquid and liquid flux in the cloud.

4. Examples of procedure for extracting drop size spectra

Figure 5 shows an example of stacked spectra of reflectivity for snow (above approximately 2100 m) and liquid water (below approximately 1900 m) on 28 September 1990 at Stapleton International Airport, Denver, Colorado (Gossard et al. 1992). The radar system has been described by Strauch et al. (1984). Its characteristics are given in Table 1. The transition from snow to liquid is often well defined (Martner and Bat-

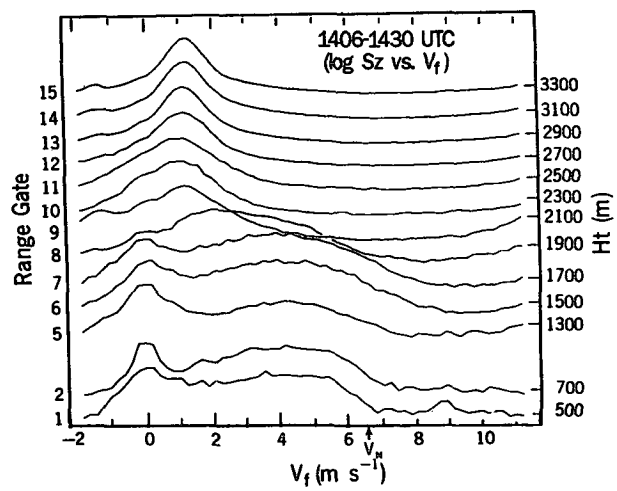

FIG. 5. Stacked spectra observed at 1406–1430 UTC 28 September 1990 by a vertically pointing, 32-cm-wavelength Doppler radar with the characteristics shown in Table 1. The spectra are plotted as logS_Z, and are all normalized to the same vertical spread. The melting level is dramatically revealed by the abrupt increase in fall velocity at a height of 1900 m. Positive velocities are downward.

TABLE 1. Stapleton Doppler radar characteristics.

Characteristic	Value
Frequency	915 MHz
Maximum bandwidth	2 MHz
Peak power	5.6 kW
Duty cycle	<25%
Antenna aperture	~10 m × 10 m
Antenna pointing	Zenith, 15° off-zenith to north and east
Antenna type	Offset paraboloidal reflector with offset horn feeds
Two-way beamwidth	1.7°
System noise temperature	240 K
Data processing	
Pulse width	1.33 μs
Gate spacing	1.33 μs
Pulse repetition period	100 μs
Average power	110 W
Time domain averaging	124 pulses
Spectral averaging	10 spectra
Maximum (folding) radial velocity	6.5 m s^{-1}
Spectral resolution (64 points)	0.203 m s^{-1}
Pulse delay	5 μs
Height sampling	
First height	0.50 km
Height spacing	200 m
Number of heights	32

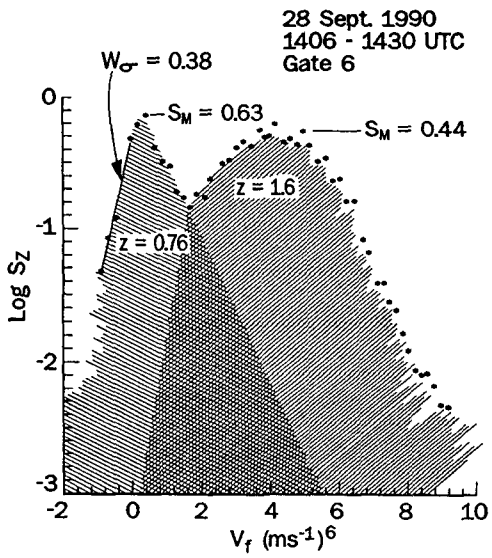

FIG. 6. The spectrum from gate 6 of Fig. 5 at a height of 1500 m, showing a precipitation peak with fairly high fall velocities and a cloud peak centered on a fall velocity of about zero. Here, Z values for the two peaks were calculated from the shaded areas. Peak maxima are shown as S_M.

tan 1962) by the increase in fall velocity during melting. In this case the spectral peak shifts from about 1.5 to 4–5 m s^{-1} during the ice–water transition. We choose the spectrum from range gate 6 (1500 m) as an example for applying the techniques described above. Figure 6 shows the spectrum to have two distinct peaks; one near $V_f = 4$ m s^{-1}, clearly associated with rain from the melted snow flakes, and one near $V_f = 0$ produced by backscatter from cloud droplets or from clear-air refractivity fluctuations or both. We now analyze both peaks using the methods described above. A least-squares fit to the five points on the left side (negative V_f) slope of the peak near zero (solid line) gives $w_\sigma = 0.38$. The values of Z (mm^6 m^{-3}) are shown for the areas under each of the two peaks. They consist of the measured Z for $V_f \geq 2$ (for the precipitation peak) and the measured Z for $V_f \leq 2$ (for the cloud–clear-air peak). A small amount was added to the Z data under the precipitation peak for $V_f < 2$ by extrapolating the precipitation data to $V_f = 0$. (It is much smaller than it appears in the figure because of the log scale.) Similarly, a small amount was added to the Z of the cloud peak by estimating the area for $V_f > 2$ using a simple exponential extrapolation of the data. Also, the peak maxima (S_M) are shown on Fig. 6. The appropriate DF is found from Fig. 4. However, when w_σ / w_M is very small, as for most precipitation spectral peaks, the figure is not resolvable; we therefore calculated DF = 1.14 from (19) and (20). However, for precipitation, DF is usually so near unity that it is seldom worth calculating. With DF = 1.14, $S_{QM} \approx 0.5$. Using these values in (32), we find, for the precipitation peak, that $w_M = 3.9$ m s^{-1}. This agrees with the Doppler-measured peak velocity on the horizontal axis of Fig. 6 within reading error. Then, converting V_f to D using (10a) and (10b), we find $D_M = 0.81$, 0.98, and 1.05 mm, respectively, for $\alpha = 0$, 1, and 2, as shown in Fig. 7. The gamma distribution curves fit the precipitation data well up to sizes of 2 mm in diameter. This example shows that

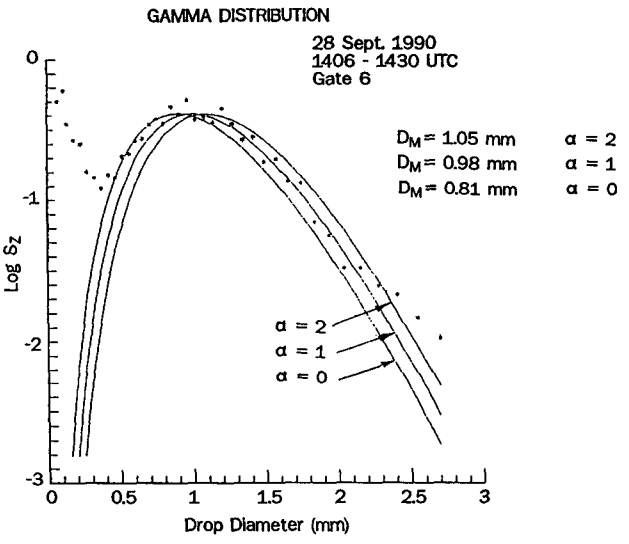

FIG. 7. The spectrum of Fig. 6 but plotted on a horizontal axis of size D rather than fall velocity. The three solid curves were found by calculating w_M with Eq. (32) and using it in Eq. (5) [written in terms of w/w_M rather than D/D_M, and using Eq. (10a)].

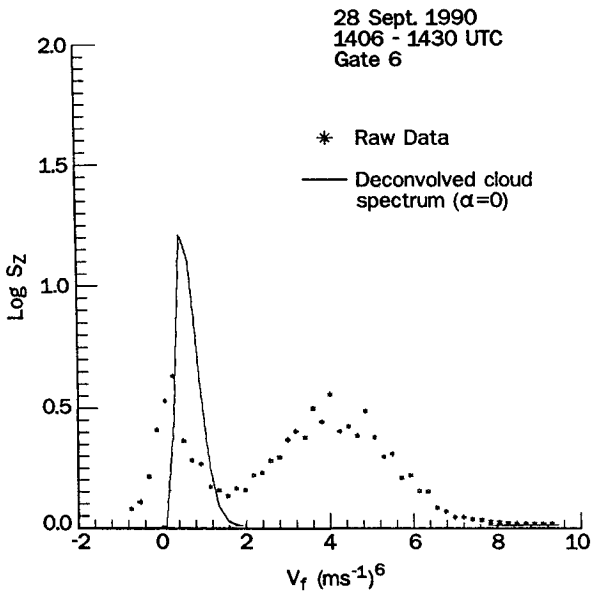

FIG. 8. The same spectrum as shown in Fig. 6 but plotted as S_Z rather than logS_Z. The deconvolved cloud spectrum for the cloud regime (solid line) is superimposed.

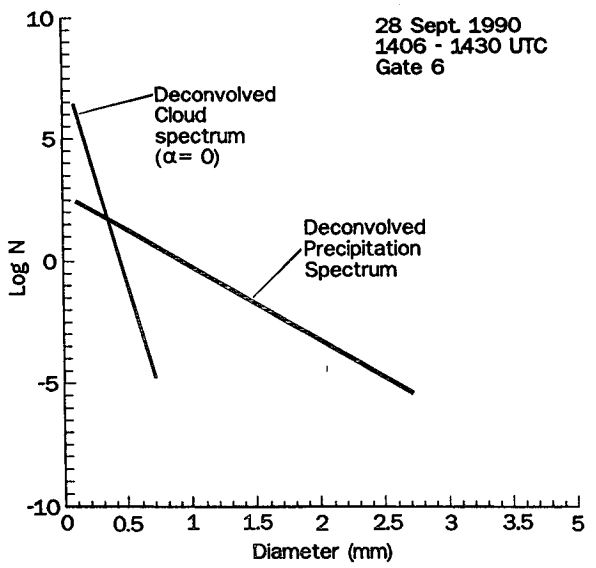

FIG. 9. Deconvolved spectra of number density assuming $\alpha = 0$, for gate 6 of Fig. 5, calculated by the method introduced in this report.

radar measurements of Z, S_M, and w_σ can be used to represent the precipitation domain of the Doppler spectrum, and it gives considerable encouragement that we can similarly represent the cloud spectrum, for which we do not have resolvable Doppler fall velocities against which to check our results. Using Z, w_M, and D_M in (26) and (27), we find LW = 2.7×10^{-3} g m^{-3} and $F_T = 6.6 \times 10^{-3}$ g m^{-2} s^{-1} for the precipitation spectral domain.

For the cloud spectral peak near $V_f = 0$, we adopt the exponential form ($\alpha = 0$) for $N(D)$. Equation (32) gives $w_M = 0.6$ m s^{-1}, which from (9) and (10) gives $D_M = 140$ μm at 850 mb, or $D_0 = 86$ μm. From Fig. 4, the deconvolution factor is 1.94. The resulting deconvolved spectrum of S_Z for the cloud peak is shown as the solid curve in Fig. 8. The resulting value of liquid water density is LW = 0.312 g m^{-3} and of liquid flux is $F_T = 0.124$ g m^{-2} s^{-1}. The total cloud drop number density $N_T = 9.3 \times 10^6$ m^{-3}. The deconvolved number density spectra for the two regimes are shown in Fig. 9 for $\alpha = 0$.

Surface airway observations at Stapleton International Airport indicate that precipitation in the form of light rain or rain showers began at the ground at about the time these spectra were recorded. The cloud system was generally stratiform, widespread, and time stationary in a mild upslope flow.

The calculated quantities are reasonable for these conditions (see Table 2), although it is perhaps surprising that such a large percentage of the flux is from the cloud spectral peak. (This is because $w_M = 0.6$ is fairly large, implying a cloud mass median radius of about $r_0 = 40$ μm, which is more representative of drizzle than typical cloud.)

Although these results seem reasonable for backscatter from liquid particles, we cannot unambiguously rule out a contribution from backscatter by refractive-index fluctuations in the medium in which the droplets are embedded. The Z value associated with the cloud peak corresponds to $C_n^2 = 3.5 \times 10^{-14}$ m$^{2/3}$, which is considerably larger than usual at heights of 1900 m, but perhaps not unreasonable for these weather conditions. Because of these uncertainties, the examples used in this paper must be considered only illustrative. It is obviously important to use at least two radars of different wavelengths to view the same volume. Since backscatter from a droplet population is proportional to λ^{-4}, whereas backscatter from refractive index fluctuations is proportional to $\lambda^{-1/3}$, the two contributions can then be unambiguously separated. Perhaps of even more importance, short-wavelength radars, such as those in the K bands, can be used even though they do not provide information about up-/downdrafts, because (32) is independent of vertical velocity in the

TABLE 2. Cloud parameters (Squires 1958).

Cloud type	Number density N_T (m^{-3})	Water content LW (g m^{-3})	Median diameter D_0 (μm)
Continental cumulus	495×10^6	0.35	13.2
Trade-wind cumulus	72.5×10^6	0.81	26.5
Hawaiian dark stratus	23.3×10^6	0.355	34.0
Hawaiian orographic	5.2×10^6	0.523	92.0

medium. In such radars the droplet backscatter will generally greatly exceed the refractive index backscatter, so little ambiguity will arise.

5. Effect of the form of the PDF on the deconvolution

A question of interest is how sensitive the deconvolution is to the form of the turbulent velocity PDF. We therefore numerically solved (12a), using the Gaussian PDF:

$$\text{PDF} = \frac{1}{(\pi w_\sigma^2)^{1/2}} \exp\left[-\left(\frac{w - w_i}{w_\sigma}\right)^2\right] \quad (33)$$

and $S_Q(w)$ again given by (5).

Figure 10 shows a plot like Fig. 4, in which a Gaussian PDF was used instead of the exponential PDF. The curve for $\alpha = 0$ is also shown in Fig. 4 (dashed) for easy comparison with the exponential PDF. The integration was carried out numerically. We note that the deconvolution factors produced by the two PDFs are similar in shape, but the Gaussian DF is smaller than that for the exponential PDF, and the curves are not so linear. The apparent differences in the results from the two PDFs are mainly due to the different normalization factors and the different meanings of w_σ (and therefore of the ratio w_σ/w_M) for the two PDFs. The solution for D_M versus Z/S_M is shown as the dashed curves in Figs. 15–17. There is some difference

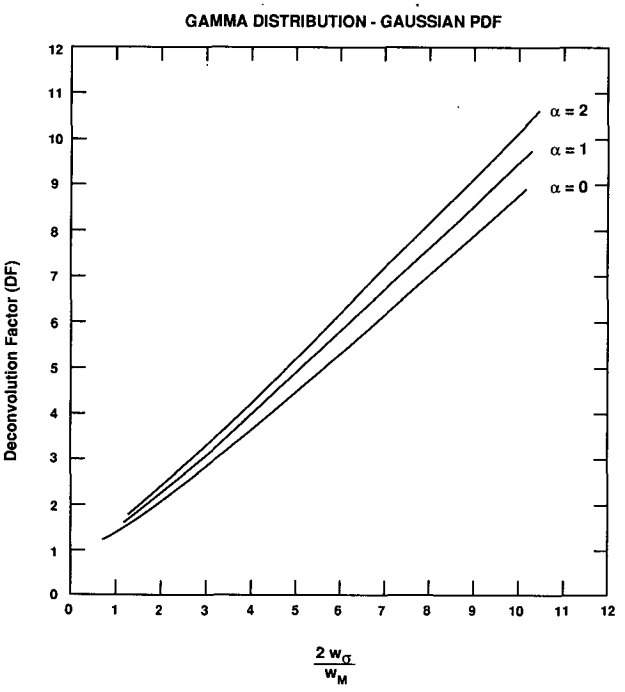

FIG. 10. Same as Fig. 4 but a Gaussian PDF [Eq. (33)] is used rather than the exponential [Eq. (11)]. The integration in Eq. (12a) was carried out numerically.

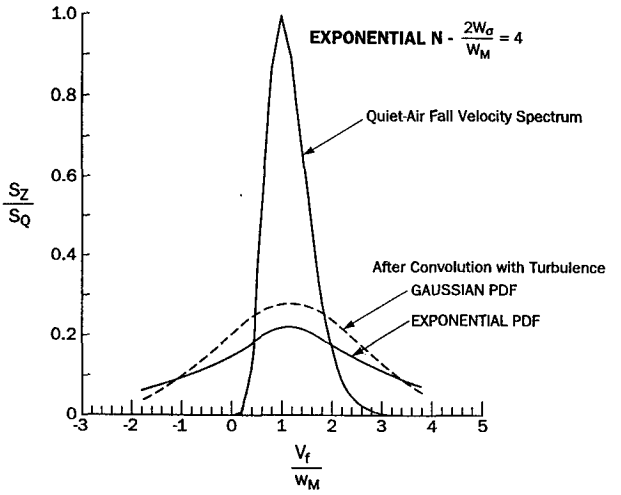

FIG. 11. Spectra calculated by assuming an exponential quiet-air number density spectrum convolved with 1) an exponential PDF and 2) a Gaussian PDF. It was assumed that $w_\sigma = 0.5$ m s^{-1}. The normalized quiet-air fall velocity spectrum is also shown.

in the spectral shape (see Fig. 11). In fact, for large deconvolution factors the spectra approach exponential and Gaussian shapes in the two respective cases. For the peak near zero on 28 September (Fig. 6), $D_M \approx 0.2$ mm for the Gaussian PDF.

6. The lognormal distribution

Another distribution function commonly used to describe cloud drop size spectra is the lognormal function (e.g., Feingold and Levin 1986). It is usually written in the form (e.g., Mason 1971)

$$N(D) = N_G \exp\left[-\frac{(\ln D - \ln D_G)^2}{2 \ln^2 \sigma_G}\right], \quad (34)$$

where N_G is the maximum of the number density spectrum, D_G is the drop diameter at the maximum, and σ_G is a width parameter. We will write the spectra of $N(D)$ and $S_Z(D)$ in terms of the reflectivity factor maximum S_M, located at D_M. Then, using (2) and using L'Hospital's rule to find the maximum of S_Z, we find

$$\ln D_M = \ln D_G + 6 \ln^2 \sigma_G, \quad (35)$$

whence, analogous to (5) and (6),

$$S_Z(D) = S_M\left(\frac{D}{D_M}\right)^6 \times \exp\left\{-3\left[\frac{\ln^2(D/D_G) - \ln^2(D_M/D_G)}{\ln(D_M/D_G)}\right]\right\} \quad (36)$$

and

$$N(D) = N_G \exp\left\{-3\left[\frac{\ln^2(D/D_G)}{\ln(D_M/D_G}\right]\right\}. \quad (37)$$

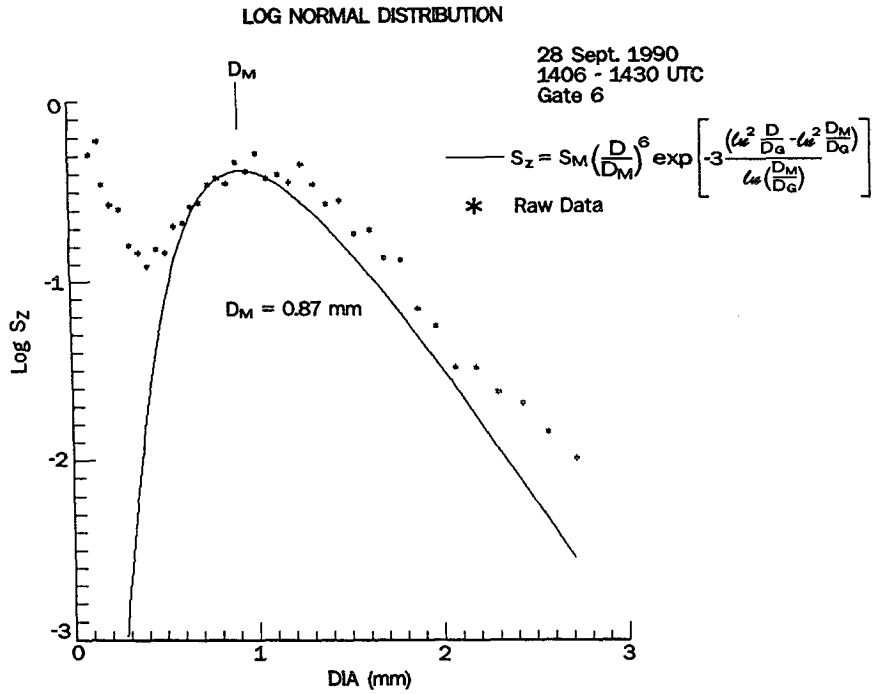

FIG. 12. Same as Fig. 7 but assuming a lognormal quiet-air number density distribution with $D_M/D_G = 1.43$ instead of a gamma distribution. The value of D_M calculated from Eq. (38) is 0.87, in good agreement with the values from the gamma functions shown in Fig. 7.

Assuming we are again interested in the size range where $w(D)$ is proportional to D, we integrate (36) to obtain Z and find, analogous to (30), that

$$Z = S_M \mathrm{DF} w_M f(y), \tag{38}$$

where $y = \ln(w_M/w_G)$ and

$$f(y) = \left(\pi \frac{y}{3}\right)^{1/2} \exp\left(\frac{y}{12}\right).$$

Using the quantities shown in Fig. 6 for Z and S_M, and assuming DF $\approx$ 1.0, as is true for the precipitation

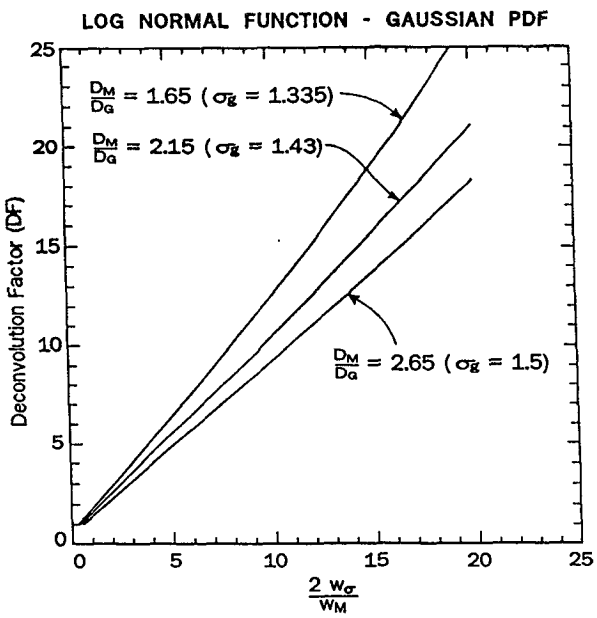

FIG. 13. Same as Fig. 4 but for a lognormal distribution like the one used in Fig. 12.

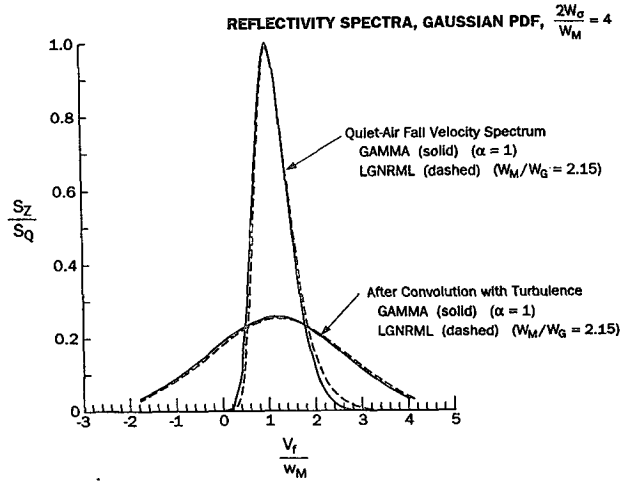

FIG. 14. Comparison of convolved reflectivity spectra for gamma quiet-air number density spectra with $\alpha = 1$ (solid) and for lognormal quiet-air spectrum $w_m/w_G = 2.15$.

TABLE 3. Viscosity μ^* (g m^{-1} s^{-1}) and density ρ_a (kg m^{-3}) of air.

T (°C)	Pressure (mb) μ	1000 ρ_a	900 ρ_a	800 ρ_a	700 ρ_a	600 ρ_a	500 ρ_a
−20	1.615×10^{-2}	1.3761	1.2385	1.1009	0.9633	0.8257	0.6881
−10	1.667×10^{-2}	1.3238	1.1915	1.0591	0.9267	0.7943	0.6619
0	1.718×10^{-2}	1.2754	1.1478	1.0203	0.8928	0.7652	0.6377
10	1.768×10^{-2}	1.2303	1.1073	0.9843	0.8612	0.7382	0.6152
20	1.818×10^{-2}	1.1884	1.0695	0.9507	0.8319	0.7130	0.5942
30	1.866×10^{-2}	1.1492	1.0343	0.9193	0.8044	0.6895	0.5746

* Kinematic viscosity $v = \mu/\rho_a$.

peak, we find w_M from (38). The resulting plot of S_Z, for $w_M/w_G = 2.15$, is shown by the solid curve in Fig. 12. This value of w_M/w_G corresponds to $\sigma_G = 1.43$, recommended by Feingold and Levin (1986). The resulting D_M is equal to 0.87 mm, which is in good agreement with the values found earlier from the gamma function (see Fig. 7). We therefore conclude that the technique is not very sensitive to the exact functional form chosen for the spectrum. Numerically solving the integral in (12a) with S_Q having the form of (36), and using the Gaussian PDF given by (33), we find the deconvolution factors for the lognormal distribution to be as shown in Fig. 13. Figure 14 compares the shape of a convolved lognormal spectrum with the corresponding gamma spectrum.

7. The Stokes range

For very small drops (less than about 100 μm), the droplet velocity relative to the medium is very small, so the dynamic interactions become negligible and the droplet rate of descent relative to the medium is described by the balance between the buoyancy force F_B and the viscous drag force F_D. The buoyancy force is

$$F_B = g\left(\frac{\pi}{6}\right)D^3(\rho_w - \rho), \tag{39}$$

where ρ is air density, ρ_w is water density, g is gravitational acceleration, and D is drop diameter. The viscous drag is the product of the force per unit area ($3\mu V_f D^{-1}$) and the surface area of the sphere (πD^2). This gives

$$F_D = 3\pi\mu V_f D, \tag{40}$$

which is the Stokes formula for viscous drag on a sphere, where μ is the molecular viscosity. Equating (39) and (40), and neglecting air density compared with water density, gives the V_f versus D relationship

$$V_f = \rho_w \frac{gD^2}{18\mu} \tag{41}$$

in the Stokes size range, where ρ_w is in grams per cubic centimeter, D is in millimeters, g is in meters per square second, μ is in grams per meter per second, and V_f is in meters per second. Data collected in a wind tunnel by Beard and Pruppacher (1969) support the reality of the Stokes range, so we next consider its possible effects on our previous results, which were based on a linear V_f versus D relationship. For the reader's convenience we have tabulated μ and ρ versus temperature and pressure in Table 3. The velocity distributions in the Stokes range are shown with those of the linear range in Fig. 1 for three pressure-height levels in a typical atmosphere using values interpolated from Table 4.

TABLE 4. Stokes range parameters.

P (mb)	μ (g m^{-1} s^{-1})	ρ (kg m^{-3})	V_S (m s^{-1})	D_S (mm)
1013	0.0179	1.213	0.53	0.130
850	0.0173	1.05	0.59	0.137
700	0.0167	0.93	0.64	0.140

We first examined a model in which the cloud droplet size and reflectivity spectra are given by (5) and (6) and in which the size versus fall velocity relations are given by (10a) and (41), joined at the common velocity

$$V_S = \frac{288\mu\rho_0}{\rho_w g\rho}, \tag{42}$$

where the common size is

$$D_S = \left(\frac{18\mu}{g}V_S\right)^{0.5}. \tag{43}$$

This led to DF and Z/S_M functions with large, unrealistic anomalies in the transitional zone between the linear and Stokes ranges because of the large discontinuity in the first derivatives of the functions where they were joined. We therefore adopted a D versus V_f function proposed by Rogers et al. (1993) that is continuous and has a first derivative that is continuous across the Stokes range interface. When modified for the effect of density, as in (10a), it is given by

$$V_f = 4\left(\frac{\rho}{\rho_0}\right)^{-0.5} D[1 - \exp(-12D)]. \tag{44}$$

For comparison with the results using the linear D versus V_f relationship, we assume the same drop size

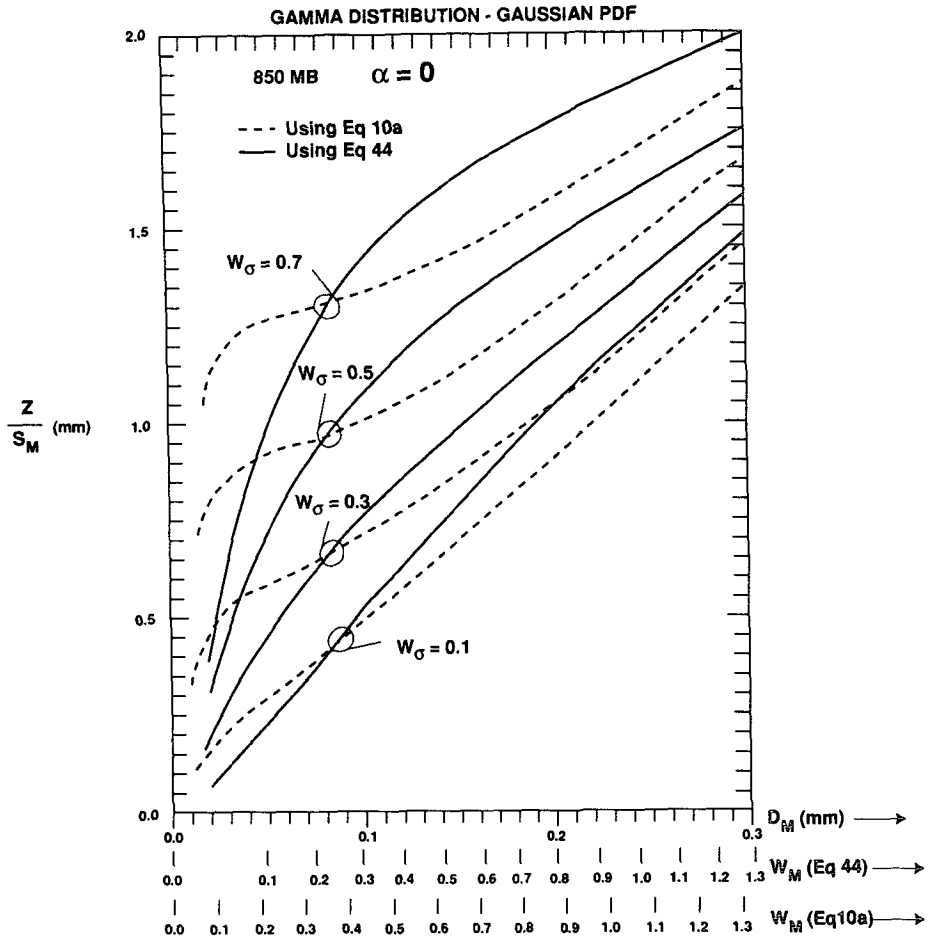

FIG. 15. Graphical solution for Z/S_M versus modal diameter of a cloud population (D_M) when a Stokes range exists [Eq. (44)] (solid) and when a linear D versus V_f relationship is assumed (dashed). The size, D_M, is the diameter at the maximum of the reflectivity spectrum S_Z, and w_M is the corresponding terminal velocity. Plots are parametric in the turbulent velocity spectral width (w_σ). Velocity scales, w_M, are superimposed for the case with a Stokes range (middle scale) and for the linear D vs V_f relation (bottom scale). Case of $\alpha = 0$.

distribution [Eq. (6)] and the same turbulent PDF [Eq. (33)] and carry out the integrations numerically in the size domain D to find DF. Then analogous to (30),

$$D_M = \frac{Z}{S_{DM}\mathrm{DF}} f(\alpha), \tag{45}$$

where S_{DM} is the maximum spectral density of the size spectrum. Because we measure the spectral density of the velocity spectrum, we must replace S_{DM} by S_M where, in the Stokes range,

$$S_{DM} = S_M \frac{dV_f}{dD}, \tag{46}$$

which when inserted in (45) gives the size parameter we want. Here, D_M is the diameter associated with the maximum of the function (5). The deconvolution factor (shown in Fig. 18) is then the same function of D as in the linear case. However, the Z/S_M functions differ when plotted versus fall velocity because of the differences between (10a) and (44) and because of the different dV_f/dD in (46). Figures 15–17 show Z/S_M (which is the quantity measured by the radar) plotted against D_M when the Stokes range is included (solid) and not included (dashed). The terminal velocities, w_M, corresponding to D_M are also shown on the horizontal axis. The plots are parametric in w_σ.

We can assess the effect of including the Stokes range by comparing the results with those assuming a linear V_f versus D relationship for the peak near zero of the 28 September spectrum analyzed earlier. For the exponential PDF, we found $w_\sigma = 0.38$. For the Gaussian PDF, (33), the equivalent w_σ is 0.43. Then from the dashed curves (linear relation) in Fig. 15, using $Z/S_M = 1.21$, we find $w_M = 0.88$ and $D_M = 0.2$ mm, and with the Stokes range included (solid)

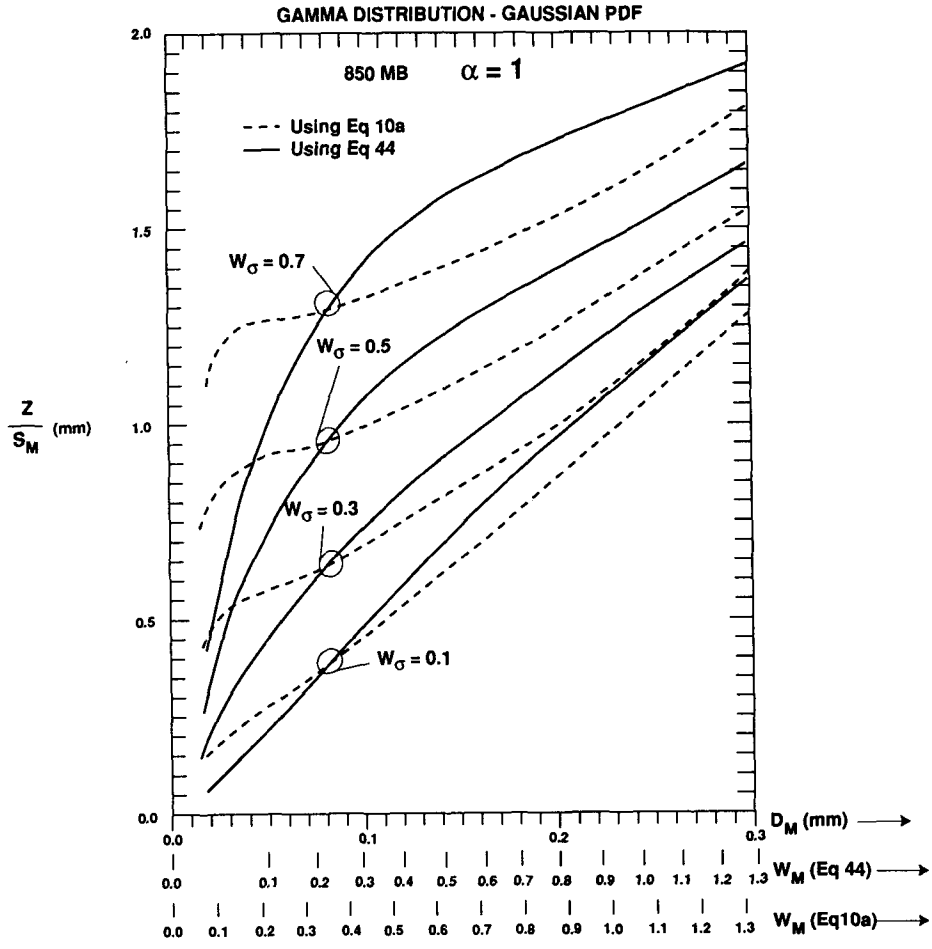

FIG. 16. Same as Fig. 15 but $\alpha = 1$.

$w_M = 0.67$ and $D_M = 0.16$ mm. Thus, in this case, when the Stokes range is included, the calculated droplet diameter is about 0.8 of that found for the simple linear relationship and a Gaussian PDF. Using (26), LW = 0.075 g m^{-3} without the Stokes range and 0.143 g m^{-3} when the Stokes range is included using (44). Inclusion of Stokes range effects is therefore important and the solid curves in Fig. 15–17 probably represent the best radar estimates of drop size in clouds. For the large terminal velocities associated with the precipitation peak, inclusion of a Stokes range has relatively little effect.

8. Conclusions and error assessment

a. Advantages of the technique

1) From measured Doppler radar spectra of clouds, one can extract cloud drop size information, even when fall velocities are too small to be directly resolvable by the radar.

2) Fall velocity and particle size information can be obtained independently of up-/downdrafts by using the spectrum shape parameter Z/S_M measurable by radar.

3) The calculation of the scale size in the droplet ensemble was fairly robust for variations in drop size distribution, as is seen by comparison of Figs. 15–17 for $\alpha = 0$–2. For example, when $\alpha = 0$, $D_M = 0.09$ if $Z/S_M = 1$ and $w_o = 0.5$, but when $\alpha = 2$, $D_M = 0.094$. However, a range of uncertainty of ±5% in size translates into an error of over 30% in liquid because the diameter is cubed in (26).

4) The technique should be applicable to cloud-sensing radars that cannot sense updrafts and downdrafts in the clear air.

b. Errors and limitations

The essence of this technique that allows the up-/downdrafts in the medium to be avoided is the explicit relationship between the spectral shape factor Z/S_M and the population size parameter, say the modal diameter, D_M, of the reflectivity spectrum. The functional form of the assumed drop size spectrum is therefore a source of error, as is w_o [see Eq. (32)]. If the assumed

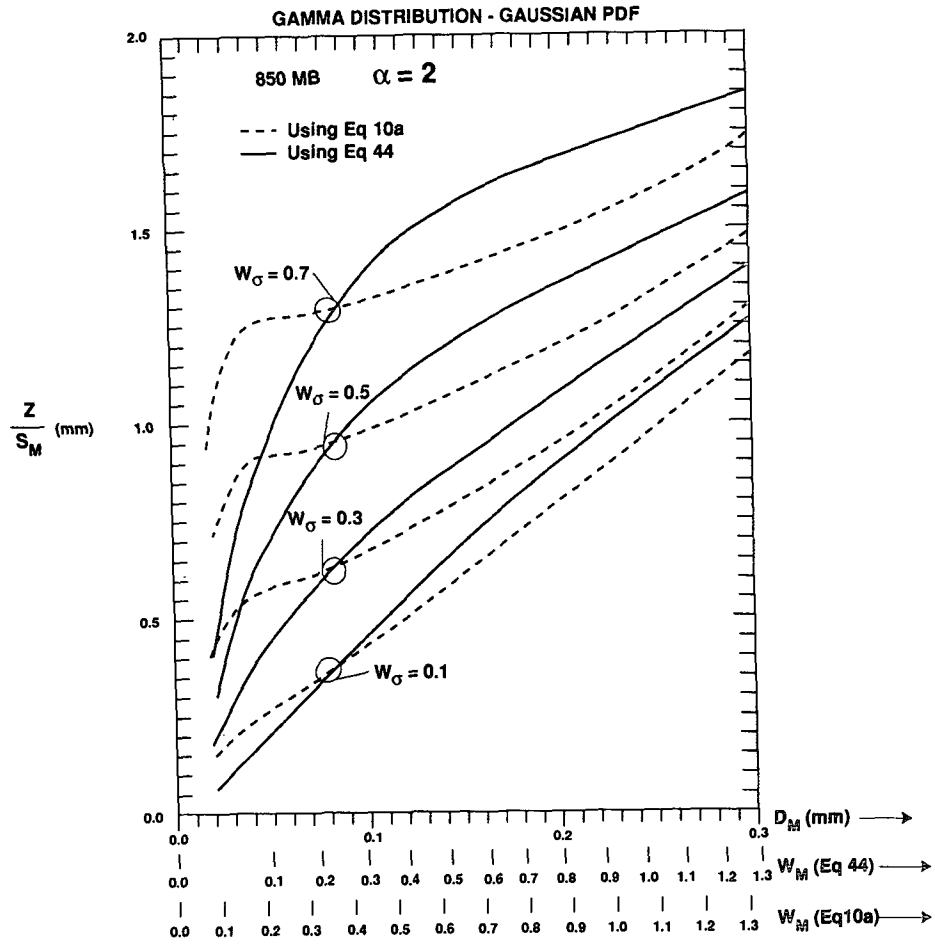

FIG. 17. Same as Fig. 15 but $\alpha = 2$.

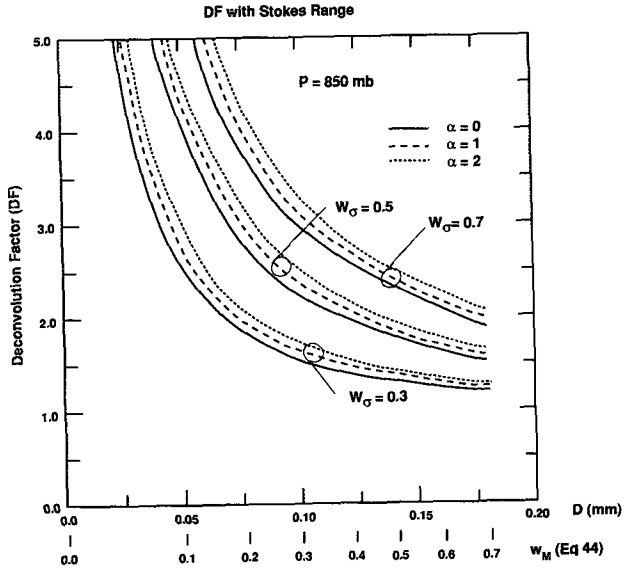

FIG. 18. Deconvolution factors for the case that includes a Stokes range.

spectral form is exactly correct with a correct w_σ, the calculated w_M will agree exactly with the correct Doppler-measured terminal velocity spectral maximum after correct removal of up-/downdrafts. The errors associated with functional form were displayed in Fig. 7, where the measured Doppler spectrum near the precipitation peak was compared with the theoretical spectra that would have resulted for various shape factors Z/S_M for gamma distributions and for the log-normal.

The calculation of scale size is quite sensitive to w_σ as seen from Figs. 15–17. For example, if $Z/S_M = 1$ and $\alpha = 0$, $D_M = 0.09$ mm if $w_\sigma = 0.5$ and $D_M = 0.15$ mm if $w_\sigma = 0.3$ because of the change in the deconvolution factor. As the turbulent velocity, w_σ, becomes larger relative to the droplet "settling velocity" w_M, greater accuracy in the measurables is needed to maintain tolerable errors in D_M. This will usually require longer integration of the observations and a uniform, steady cloud system. Longer observations in space or time lead to larger measured variances because the longer observations include contributions from larger

scales, so w_σ increases with observation time resulting in a systematic error. Such errors can be mostly removed if frequency f and wavenumber k spectra of turbulence are assumed to follow some reasonable law such as $k^{-5/3}$ and $f^{-5/3}$, but the averaging problem will require careful attention as the technique is extended to very small drops.

9. Plans and recommendations

Clearly, this technique should be evaluated using short-wavelength (e.g., 8 mm) radars that are much more sensitive to small particulates than are the profiler wavelengths. The main advantages of the profilers has been their ability to independently sense up-/downdrafts. This ability is not needed with the proposed technique, and 8-mm radars should very effectively observe drop size distributions and droplet growth in some stratus clouds (e.g., as the clouds approach a drizzle condition). (The profiler wavelengths sense the precipitation particles much more strongly than the cloud particles, and there is insufficient dynamic range in the spectral processing to sense clouds when there is substantial precipitation.)

The estimated error in cloud liquid from this radar technique can be quite large if D_M is in error, because D_M is cubed in (26), so supporting measurements of total cloud liquid by a microwave radiometer will be important to future experiments. Such measurements would provide a useful constraint on the radar-measured liquid profiles, and possibly improve the functional description of cloud drop size distributions. Direct comparison with in situ measurements of drop size spectra from aircraft are also urgently needed.

Acknowledgments. The author acknowledges important discussions and suggestions for improving the manuscript by Drs. R. Doviak, C. W. Fairall, G. Feingold, Steen Hansen, C. Knight, B. Martner, M. Politovich, R. G. Strauch, B. Stankov, R. Rogers, and T. Uttal. The work reported here was supported by the Wave Propagation Laboratory/NOAA and the Naval Command Control and Ocean Surveillance Center, Dr. J. H. Richter, Contract Monitor.

REFERENCES

Atlas, D., 1953: Optical extinction by rainfall. *J. Meteor.*, **10,** 486–489.

——, R. C. Srivastava, and R. S. Sekon, 1973: Doppler radar characteristics of precipitation at vertical incidence. *Rev. Geophys. Space Phys.*, **11,** 1–35.

Beard, K. V., 1985: Simple altitude adjustments to raindrop velocities for Doppler radar analysis. *J. Atmos. Oceanic Technol.*, **2,** 468–471.

——, and H. R. Pruppacher, 1969: A determination of the terminal velocity and drag by means of a wind tunnel. *J. Atmos. Sci.*, **26,** 1066–1072.

Doviak, R. J., and D. S. Zrnić, 1984: *Doppler Radar and Weather Observations.* Academic Press, 458 pp.

Feingold, G., and Z. Levin, 1986: The log normal fit to raindrop spectra from frontal convective clouds in Israel. *J. Climate Appl. Meteor.*, **25,** 1346–1363.

Foote, G. B., and P. S. du Toit, 1969: Terminal velocity of raindrops aloft. *J. Appl. Meteor.*, **8,** 249–253.

Gossard, E. E., and R. G. Strauch, 1983: *Radar Observations of Clear Air and Clouds.* Elsevier, 280 pp.

——, and ——, 1989: Further guide for the retrieval of dropsize distributions in water clouds with a ground-based clear-air-sensing Doppler radar. Tech. Document, NOAA/ERL/Wave Propagation Laboratory, Boulder, CO, 48 pp.

——, and ——, 1990: The retrieval of dropsize distributions in water clouds from ground-based, clear-air-sensing Doppler radar observations. *Meteor. Rundsch.* **42,** 165–173.

——, ——, and R. R. Rogers, 1990: Evolution of dropsize distributions in liquid precipitation observed by ground-based Doppler radar. *J. Atmos. Oceanic Technol.*, **7,** 815–828.

——, ——, D. C. Welsh, and S. Y. Matrosov, 1992: Cloud layers, particle identification, and rain-rate profiles from ZRV_f measurements by clear-air Doppler radars. *J. Atmos. Oceanic Technol.*, **9,** 108–119.

Gunn, R., and G. D. Kinzer, 1949: The terminal velocity of fall for water droplets in stagnant air. *J. Meteor.*, **6,** 243–248.

Marshall, J. S., and W. M. K. Palmer, 1948: The distribution of raindrops with size. *J. Meteor.*, **5,** 165–166.

Martner, B. F., and L. J. Battan, 1962: Calculations of Doppler radar velocity spectrum parameters for a mixture of rain and hail. *J. Appl. Meteor.*, **15,** 491–498.

Mason, B. J., Ed., 1971: *The Physics of Clouds.* Clarendon Press, 659 pp.

Pearson, K., Ed., 1951: *Tables of Incomplete Γ-Function.* Cambridge University Press, 164 pp.

Rogers, R. R., and M. K. Yau, 1989: *A Short Course in Cloud Physics.* Pergamon Press, 293 pp.

——, D. Baumgardner, S. A. Ethier, D. A. Carter, and W. L. Eklund, 1993: Comparison of raindrop size distributions measured by radar wind profiler and by airplane. *J. Appl. Meteor.*, **32,** 694–699.

Squires, P., 1958: The microstructure and colloidal stability of warm clouds. *Tellus,* **10,** 256–261.

Strauch, R. G., D. A. Merritt, K. P. Moran, K. B. Earnshaw, and D. van de Kamp, 1984: The Colorado wind-profiling network. *J. Atmos. Oceanic Technol.*, **1,** 37–49.

Wakasugi, K., A. Mizutani, S. Fukao, and S. Kato, 1986: A direct method for deriving dropsize distribution and vertical air velocities from VHF Doppler radar spectra. *J. Atmos. Oceanic Technol.*, **3,** 623–629.